J|A|C|S ARTICLES

Published on Web 10/21/2009

Deciphering Low Energy Deactivation Channels in Adenine

Irene Conti,[†] Marco Garavelli,*[,†] and Giorgio Orlandi*[,†,‡]

Dipartimento di Chimica 'G. Ciamician', Universita' di Bologna, Via F. Selmi, 2, 40126 Bologna, Italy, and INSTM, UdR Bologna, Italy

Received March 24, 2009; E-mail: marco.garavelli@unibo.it; giorgio.orlandi@unibo.it

Abstract: The radiationless decay paths of 9H-adenine in its lowest excited states $^1n\pi^*$, $^1L_b(^1\pi\pi^*)$, and $^1L_a(^1\pi\pi^*)$ and in dissociative $^1\pi\sigma^*$ states have been mapped in vacuo at the CASPT2//CASSCF resolution. The minimum energy path (MEP) of the ^1L_a state, which shows the strongest absorption below 5 eV, is found to decrease monotonically along the puckering coordinate from the vertical excitation to a $S_0/^1L_a$ conical intersection (CI). The vertically excited $^1n\pi^*$ and ^1L_b states are found to relax to the respective minima and to require some energy to reach CIs with S_0. This picture suggests that ^1L_a alone is responsible of both components of the ultrafast biexponential decay (with $\tau_1 < 0.1$ ps and $\tau_2 < 1$ ps) recently observed in time-resolved pump−probe resonant ionization and fluorescence spectroscopy, and that the $^1n\pi^*$ and ^1L_b states do not act as important intermediates in the ^1L_a decay process. We find that the $^1L_a \rightarrow {}^1\pi\sigma_{N9H}^*$ internal conversion can be followed by N_9-H photocleavage, albeit with tiny quantum yield. The amino $N_{10}-H$ bond photocleavage is hindered by the high barrier encountered along the $N_{10}-H$ bond-breaking path in the $^1\pi\sigma_{N10H}^*$ state.

1. Introduction

DNA bases show a remarkable degree of photostability that is essential for the preservation of the genetic information. Their photophysical properties have been discussed in many contributions,[1−4] and the ultrafast dynamics of their excited states, which return back to the reactant ground state much faster than other competing and damaging photoreactions, have been reviewed recently by Kohler and co-workers.[5,6] In this paper we consider the dominant 9H isomer of adenine (Ade), which is shown in Scheme 1.

In vapor, the Ade absorption spectrum shows two bands[1] with maxima at 249 and 207 nm, assigned to the ^1L_a and ^1B_b $^1\pi\pi^*$ singlet excited states, respectively. In solution, the two bands are slightly red-shifted.[7,8]

In the gas phase, the lowest excited singlet states of Ade are a $^1n\pi^*$ state and the two ^1L_b and ^1L_a $^1\pi\pi^*$ states.[1] The ^1L_a state has the largest transition moment to the ground state, S_0, and is responsible of most of the absorption in the spectral region below 5 eV. Furthermore, low-lying $^1\pi\sigma^*$ states, where σ^* is the antibonding orbital localized on a N−H bond, which are not observed in the optical spectra, are in the same energy range of ^1L_a according to recent CASSCF and TDDFT calculations.[9−16] Molecular beam spectra of Ade[17−23] obtained by resonance

Scheme 1

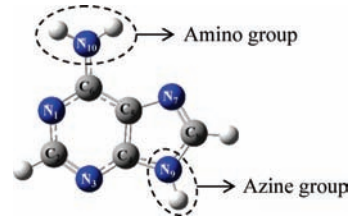

[†] Universita' di Bologna.
[‡] INSTM.

(1) Clark, L. B.; Peschel, G. G.; Tinoco, I. *J. Phys. Chem.* **1965**, *69*, 3615.
(2) Callis, P. R. *Annu. Rev. Phys. Chem.* **1983**, *34*, 329.
(3) Daniels, M. *Photochemistry and Photobiology of Nucleic Acids*; Academic Press: New York, 1976; Vol. 1, p 23.
(4) Cadet, J.; Vigny, P., *Bioorganic Photochemestry.*; Wiley: New York, 1990; Vol. 1, p 1.
(5) Crespo-Hernandez, C. E.; Cohen, B.; Hare, P. M.; Kohler, B. *Chem. Rev.* **2004**, *104*, 1977.
(6) Middleton, C. T.; de La Harpe, K.; Su, C.; Law, Y. K.; Crespo-Hernãndez, C. E.; Kohler, B. *Annu. Rev. Phys. Chem.* **2009**, 60.
(7) Voet, D.; Gratzer, W. B.; Cox, R. A.; Doty, P. *Biopolymers* **1963**, *1*, 193.
(8) Clark, L. B.; Peschel, G. G.; Tinoco, I. *J. Am. Chem. Soc.* **1965**, *87*, 11.
(9) Sobolewski, A. L.; Domcke, W.; Dedonder-Lardeux, C.; Jouvet, C. *Phys. Chem. Chem. Phys.* **2002**, *4*, 1093.
(10) Sobolewski, A. L.; Domcke, W. *Eur. Phys. J. D* **2002**, *20*, 369.
(11) Perun, S.; Sobolewski, A. L.; Domcke, W. *Chem. Phys.* **2005**, *313*, 107.
(12) Ritze, H. H.; Lippert, H.; Samoylova, E.; Smith, V. R.; Hertel, I. V.; Radloff, W.; Schultz, T. *J. Chem. Phys.* **2005**, *122*, 224320.
(13) Yamazaki, S.; Kato, S. *J. Am. Chem. Soc.* **2007**, *129*, 2901.
(14) Chung, W. C.; Lan, Z.; Ohtsuki, Y.; Shimakura, N.; Domcke, W.; Fujimura, Y. *Phys. Chem. Chem. Phys.* **2007**, *9*, 2075.
(15) Marian, C. M. *J. Chem. Phys.* **2005**, *122*, 104314.
(16) Satzger, H.; Townsend, D.; Zgierski, M. Z.; Patchkovskii, S.; Ullrich, S.; Stolow, A. *Proc. Natl. Acad. Sci. U.S.A.* **2006**, *103*, 10196.
(17) Kim, N. J.; Jeong, G.; Kim, Y. S.; Sung, J.; Kim, S. K.; Park, Y. D. *J. Chem. Phys.* **2000**, *113*, 10051.
(18) Lührs, D. C.; Viallon, J.; Fischer, I. *Phys. Chem. Chem. Phys.* **2001**, *3*, 1827.
(19) Plützer, C.; Nir, E.; de Vries, M. S.; Kleinermanns, K. *Phys. Chem. Chem. Phys.* **2001**, *3*, 5466.
(20) Plützer, C.; Kleinermanns, K. *Phys. Chem. Chem. Phys.* **2002**, *4*, 4877.
(21) Kim, N. J.; Kang, H.; Park, Y. D.; Kim, S. K. *Phys. Chem. Chem. Phys.* **2004**, *6*, 2802.
(22) Nir, E.; Kleinermanns, K.; Grace, L.; de Vries, M. S. *J. Phys. Chem. A* **2001**, *105*, 5106.
(23) Nir, E.; Pltzer, C.; Kleinermanns, K.; de Vries, M. *Eur. Phys. J. D* **2002**, *20*, 317.

 10.1021/ja902311y CCC: $40.75

enhanced two-photon ionization (R2PI) and laser-induced fluorescence (LIF) showed a number of resolved vibronic bands (labeled A, C, D, E) in the region from 4.40 to about 4.55 eV, interpreted as ^1L_b and $^1n\pi^*$ vibrational levels, followed by a broad continuous absorption above 4.55 eV, associated with the $S_0 \rightarrow {}^1L_a$ transition.[17−23]

The lifetime of Ade excited to the band D in molecular beams was found by Lührs et al.[18] to be ≈9 ps and was subsequently estimated to be about 40−50 ps from Lorentzian linewidths of the rovibronic transitions.[24,25] Lifetimes obtained by excitation in the broad UV absorption continuum with $\lambda < 272$ nm are much shorter.[26,27] In particular, time-resolved photoelectron spectroscopy (TRPES) measures[16,28−30] identified two distinct processes with lifetimes $\tau_1 \approx 0.05$ and $\tau_2 \approx 0.75$ ps, exciting both with light wavelengths of $\lambda = 250$ and 267 nm (4.96 and 4.64 eV). Slightly different pump and probe techniques, using 267, 263, and 250 nm excitation wavelengths, confirmed a biexponential decay for gas phase Ade with $\tau_1 \approx 0.1$ and $\tau_2 \approx$ 1.1 ps time constants.[31] Also, excitation with 272 nm (4.56 eV) photons leads to a biexponential decay with the same τ_1, 0.1 ps, but a slightly longer τ_2 (2.3 ps).[32] These results indicate that the nonradiative dynamics of Ade depends critically on the excitation energy: the lifetimes at excitation wavelengths above 272 nm become longer as the wavelength increases.

The shorter (≈0.1 ps) lifetime is generally attributed to the internal conversion (IC) decay of ^1L_a directly to S_0[33−35] or to the lower excited states $^1n\pi$, ^1L_b and, if enough energy is available, to $^1\pi\sigma^*$.[11,28−30,35−38] The longer lifetime (≈1 ps) is assumed to represent the subsequent decay of the latter states to S_0.

In solutions, the energy gap and the ordering of the lowest Ade excited states may change with respect to gas phase[12,13,39,40] and, consequently, the excited states lifetime and decay mechanisms may be affected by solvation. Ade aqueous solutions were studied by time-resolved fluorescence[37,41] and transient absorption[42,43] experiments. The recent time-resolved measures of Ade in water, performed by Phillips and co-workers[44] by exciting at 267 nm, revealed a biexponential decay with time constants 0.13 and 0.45 ps, very similar to the lifetimes obtained in gas phase.[16,28,30−32] A similar τ_1 result (0.23 ps) was obtained in ref 41. These results are in agreement with correlated pump and probe studies on Ade$(H_2O)_n$ water clusters.[12,45] The same experiments[31] on 9M-Ade$(H_2O)_n$ clusters yielded a biexponential decay with both lifetimes decreasing from $\tau_1 \approx 0.11$ and $\tau_2 \approx$ 1.3 ps for $n = 0$ (gas phase) to $\tau_1 \approx 0.10$ and $\tau_2 \approx 0.75$ ps for $n = 6$.[31] The comparison between the lifetimes of Ade and 9M-Ade in gas phase versus in water suggests that the two decay processes do not depend on states, like $^1n\pi^*$, that are subject to solvent perturbations.

The ^1L_a deactivation route via $^1\pi\sigma_{NH}^*$ states received wide theoretical[9−16] and experimental[24,46,47] attention, because it leads to the potentially dangerous N−H bond photocleavage and radical formation. Although this process should be sensitive to deuteration, the decay times of three deuterated Ades were found by the Kim group[27] (exciting at 267 nm) virtually identical to undeuterated Ade (≈1 ps). The absence of deuterium effect on the 1 ps decay constant rules out the possibility that at this excitation wavelengths the decay of ^1L_a via $^1\pi\sigma_{NH}^*$ states is an appreciable decay path. Rather, it may represent only a minor channel that is manifested only by the N−H bond fission with production of H atoms.[24,46,47] In fact, several studies have reported H atom production by exciting the ^1L_a absorption band of Ade down to 266 nm (4.66 eV)[46] and 243.1 nm (5.10 eV).[24] However, the observed fragmentation may occur not only by N−H photocleavage[47] induced by the ^1L_a excitation, but also by bond breaking occurring on the vibrationally excited S_0, following internal conversion.[47] Currently, the lower energy excitation for obtaining the N−H photocleavage, following the ^1L_a excitation and the $^1L_a \rightarrow {}^1\pi\sigma_{N10H}^*$ and $^1L_a \rightarrow {}^1\pi\sigma_{N9H}^*$ fast internal conversions, has been put at 233 nm (5.32 eV).[47] By comparison, the energy of the lowest $^1\pi\sigma_{NH}^*/{}^1L_a$ conical intersection was computed at about 5.3 eV[11,15] and the $^1\pi\sigma_{N9H}^*$ ($^1\pi\sigma_{N10H}^*$) energies at the local minimum and were estimated 4.90 (4.91) eV.[12]

The Ade excited states and their fast radiationless decays have been extensively studied by theoretical approaches mostly based on the search of conical intersections (CIs) between different electronic states.[9−16,33−36,38−40,48−56] The decay channels for

(24) Hünig, I.; Pltzer, C.; Seefeld, K. A.; Lwenich, D.; Nispel, M.; Kleinermanns, K. *ChemPhysChem* **2004**, *5*, 1427.
(25) Lee, Y.; Schmitt, M.; Kleinermanns, K.; Kim, B. *J. Phys. Chem. A* **2006**, *110*, 11819.
(26) Kang, H.; Lee, K. T.; Jung, B.; Ko, Y. J.; Kim, S. K. *J. Am. Chem. Soc.* **2002**, *124*, 12958.
(27) Kang, H.; Jung, B.; Kim, S. K. *J. Chem. Phys.* **2003**, *118*, 6717.
(28) Ullrich, S.; Schultz, T.; Zgierski, M. Z.; Stolow, A. *J. Am. Chem. Soc.* **2004**, *126*, 2262.
(29) Bisgaard, C. Z.; Satzger, H.; Ullrich, S.; Stolow, A. *ChemPhysChem* **2009**, *10*, 101.
(30) Ullrich, S.; Schultz, T.; Zgierski, M. Z.; Stolow, A. *Phys. Chem. Chem. Phys.* **2004**, *6*, 2796.
(31) Canuel, C.; Mons, M.; Piuzzi, F.; Tardivel, B.; Dimicoli, I.; Elhanine, M. *J. Chem. Phys.* **2005**, *122*, 074316.
(32) Samoylova, E.; Lippert, H.; Ullrich, S.; Hertel, I. V.; Radloff, W.; Schultz, T. *J. Am. Chem. Soc.* **2005**, *127*, 1782.
(33) Serrano-Andrés, L.; Merchán, M.; Borin, A. C. *Chem.—Eur. J.* **2006**, *12*, 6559.
(34) Serrano-Andrés, L.; Merchán, M.; Borin, A. C. *Proc. Natl. Acad. Sci. U.S.A.* **2006**, *103*, 8691.
(35) Blancafort, L. *J. Am. Chem. Soc.* **2006**, *128*, 210.
(36) Chen, H.; Li, S. *J. Phys. Chem. A* **2005**, *109*, 8443.
(37) Pancur, T.; Schwalb, N. K.; Renth, F.; Temps, F. *Chem. Phys.* **2005**, *313*, 199.
(38) Perun, S.; Sobolewski, A. L.; Domcke, W. *J. Am. Chem. Soc.* **2005**, *127*, 6257.
(39) Mennucci, B.; Toniolo, A.; Tomasi, J. *J. Phys. Chem. A* **2001**, *105*, 4749.
(40) Mishra, S. K.; Shukla, M. K.; Mishra, P. C. *Spectrochim. Acta, Part A* **2000**, *56*, 1355.
(41) Gustavsson, T.; Sharonov, A.; Onidas, D.; Markovitsi, D. *Chem. Phys. Lett.* **2002**, *356*, 49.
(42) Cohen, B.; Hare, P. M.; Kohler, B. *J. Am. Chem. Soc.* **2003**, *125*, 13594.
(43) Cohen, B.; Crespo-Hernández, C. E.; Kohler, B. *Faraday Discuss.* **2004**, *127*, 137.
(44) Kwok, W.-M.; Ma, C.; Phillips, D. L. *J. Am. Chem. Soc.* **2006**, *128*, 11894.
(45) Canuel, C.; Elhanine, M.; Mons, M.; Piuzzi, F.; Tardivel, B.; Dimicoli, I. *Phys. Chem. Chem. Phys.* **2006**, *8*, 3978.
(46) Zierhut, M.; Roth, W.; Fischer, I. *Phys. Chem. Chem. Phys.* **2004**, *6*, 5178.
(47) Nix, M. G. D.; Devine, A. L.; Cronin, B.; Ashfold, M. N. R. *J. Chem. Phys.* **2007**, *126*, 124312.
(48) Nielsen, S. B.; Solling, T. I. *ChemPhysChem* **2005**, *6*, 1276.
(49) Matsika, S. *J. Phys. Chem. A* **2004**, *108*, 7584.
(50) Matsika, S. *J. Phys. Chem. A* **2005**, *109*, 7538.
(51) Ismail, N.; Blancafort, L.; Olivucci, M.; Kohler, B.; Robb, M. A. *J. Am. Chem. Soc.* **2002**, *124*, 6818.
(52) Merchan, M.; Serrano-Andres, L. *J. Am. Chem. Soc.* **2003**, *125*, 8108.
(53) Zgierski, M. Z.; Patchkovskii, S.; Fujiwara, T.; Lim, E. C. *J. Phys. Chem. A* **2005**, *109*, 9384.
(54) Chen, H.; Li, S. *J. Chem. Phys.* **2006**, *124*, 154315.
(55) Barbatti, M.; Lischka, H. *J. Am. Chem. Soc.* **2008**, *130*, 6831.
(56) Lei, Y.; Yuan, S.; Dou, Y.; Wang, Y.; Wen, Z. *J. Phys. Chem. A* **2008**, *112*, 8497.

^1L_a that have been suggested by ab initio calculations include (i) the direct decay from the excited ^1L_a state,[11,13,14,33−35,38,55] which would lead to a lower energy $^1L_a/S_0$ CI by a barrierless route along a ring-puckering coordinate; (ii) the decay of ^1L_a through the $^1n\pi^*$ or ^1L_b states, reached by ^1L_a internal conversion;[11,13,15,33−36,38,56] and (iii) the ^1L_a decay path via a $^1\pi\sigma_{N9H}^*$ ($^1\pi\sigma_{N10H}^*$) state leading to the dissociation of an N−H bond.[9−16]

Despite the large amount of valuable experimental data available for Ade and wealth of accurate theoretical calculations,[9−16,33−36,38−40,48−56] the detailed mechanisms governing the decay of Ade lowest excited states, in particular, of the path associated with the $\tau_2 \approx 1$ ps lifetime, are still not fully understood. In this work, to elucidate these processes, we have investigated the energy profiles for excited state relaxation paths for Ade in vacuo by high level ab initio correlated (CASPT2) methods. Our purpose is to assess the efficiency of all the processes discussed earlier by a *unified and computationally homogeneous treatment*. Specifically, our aim is (a) to elucidate the minimum energy paths (MEPs) following the excitation to $^1L_a(^1\pi\pi^*)$ and to assess whether internal conversions to ^1L_b and $^1n\pi^*$ states is important; (b) to examine the decay routes of the lowest ^1L_b and $^1n\pi^*$ excited states, including possible intersystem crossing (ISC) to quasi-degenerate triplet states; and (c) to ascertain the feasibility of the ^1L_a decay via $^1\pi\sigma_{N9H}^*$ and $^1\pi\sigma_{N10H}^*$ excited states.

Finally, by comparing our theoretical results with the information obtained from spectroscopic and ultrafast time-resolved experiments we try to construct a coherent picture of the photophysical/photochemical behavior of Ade.

2. Computational Details

2.1. Computational Methods. Equilibrium geometries and photoreaction paths were determined by using fully unconstrained optimizations and minimum energy path (MEP)[57,58] computations on the relevant potential energy surface (PES), respectively. Optimized geometries and MEPs are obtained at the CASSCF level, and at these geometries, the CASPT2 energy corrections are added to the CASSCF energies.[59] The standard 6-31+G** basis is used in this work; the p functions added to hydrogen atoms with this choice provide a better σ^* orbitals description. Gaussian03[60] and the MOLCAS-6.2[61] suite of programs have been employed.

Most CASSCF geometry optimizations were performed by a 12 electrons, 11 orbitals active space, in short CAS(12,11). The 11 orbitals are the 2 lone pairs on nitrogen atoms in the pyrimidine ring, 4 π orbitals, 4 π^* and 1 σ^* orbital, or, alternatively, 3 π^* and 2 σ^* orbitals, namely, the σ_{N9H}^* and σ_{N10H}^* antibonding orbitals localized on the N_9−H and N_{10}−H bonds (see Scheme 1 for atom numbering). For the calculation of the ^1L_a IRC a (12,10) active space was used, where the 10 orbitals are π and π^*, to avoid the problems arising from the contamination of ^1L_a with $n\pi^*$, $n\sigma^*$, and $p\sigma^*$ states. Furthermore, energies of the ^1L_a MEP and $n\pi^*$ and ^1L_b minima have been recomputed also with a CAS(12,9) active space (see section 2.2 below for details).

To avoid root-flipping problems, state average calculations by equally weighting the first nine roots (CASSCF/6-31+g**-SA-9) were generally employed to optimize excited state geometries. The N−H photoclevage process (section 3.4) was explored by using a 13 roots state-averaging approach (CASSCF/6-31+g**-SA-13), thus including also higher lying states such as B_b and $n\sigma^*$ states.

To avoid the problem of intruder states, an "imaginary shift"[62] value of 0.25 au was used in all CASPT2 calculations. Transition dipole moments were computed by using the CASSCF state interaction (CASSI)[63] programs of MOLCAS-6.2[61] and oscillator strengths values were evaluated by use of CASPT2 excitation energies.

2.2. Active Space Selection. Around the S_0 equilibrium structure, at the CASSCF(12,11), level two $^1n\sigma^*$ states appear at a slightly lower energy than ^1L_a. Although the CASPT2 treatment establishes the correct energy ordering, the CASSCF wave functions overestimate the mixing between ^1L_a and $^1n\sigma^*$ states. This is shown by the too low $S_0 \rightarrow {}^1L_a$ oscillator strength (0.08 vs the observed value of 0.24,[1] see Table S1 and Supporting Information) and by the overestimate of the $S_0 \rightarrow {}^1n\sigma^*$ oscillator strength. These anomalies are accompanied by an unsatisfactory energy profile of ^1L_a: the ^1L_a CASPT2//CASSCF(12,11) MEP shows a barrier (see section 3.3) that is incompatible with the observed subpicosecond ^1L_a lifetimes and is in contrast with previous calculations.[33−35] Thus, it is apparent that within the CASSCF(12,11) active space, ^1L_a is not described on the same accuracy as the other states.

To circumvent in part this difficulty we have followed two ways: (a) we performed the multistate PT2 (MSPT2) treatment,[64,65] which mixes the CASSCF wave functions at the PT2 level, and corrects the energies; (b) we run a second CASPT2//CASSCF calculation utilizing a smaller CAS(12,9) active space excluding the σ_{N9H}^* and σ_{N10H}^* to eliminate the $^1n\sigma_{N9H}^*$ and $^1n\sigma_{N10H}^*$ configurations that incorrectly mix up and perturb the ^1L_a state.

The MSPT2//CASSCF(12,11) and the CASPT2//CASSCF(12,9) calculations give similar energy results and yield a ^1L_a MEP that is lower by about 10 kcal/mol than the CASPT2//CASSCF(12,11) MEP, and that better accounts for the ^1L_a observed properties. On the contrary, the energy curves of the other electronic states, in particular, of the ^1L_b and $^1n\pi^*$ states, tend to remain unchanged.

2.3. Estimate of Radiationless Transitions Rate Constants. Let the $\Psi_{A,0} = \Phi_A \cdot \Lambda_0$, the ground vibrational state of the electronic state A, be the initial state and $\Psi_{B,v} = \Phi_B \cdot \Lambda_v$, a vibrationally excited state v of a lower electronic state B, the final state. The rate constant k (s^{-1}) of the $\Psi_{A,0} \rightarrow \Psi_{B,v}$ transition induced by $V_{A,B}$ is given by the Fermi golden rule[66]

$$k(s^{-1}) = \{[(2\pi)^2/h]V_{A,B}{}^2\} \cdot F\rho \qquad (1)$$

where F is the averaged Franck−Condon (FC) factor $<0/v>^2$ over the density ρ of vibrational states B,v that are degenerate with the state A,0, and $V_{A,B}$ is the interaction V between Φ_A and Φ_B.

While the electronic coupling $V_{A,B}$, be it vibronic or spin−orbit, can be computed, the evaluation of the $F\rho$ is very complicated for the enormous density of states. We evaluated this factor following Siebrand energy gap law of displaced harmonic oscillator[67,68] and the semiempirical expression proposed later in books.[69,70] Expressing E in eV units, we used a combination of two equations valid in two different energy gap intervals, precisely

$$F(E) = \exp(-\gamma) \cdot \gamma^v/v! \quad \text{with } v = E/0.17 \quad \text{for } E < 0.51\text{eV} \qquad (2a)$$

(57) Celani, P.; Robb, M. A.; Garavelli, M.; Bernardi, F.; Olivucci, M. *Chem. Phys. Lett.* **1995**, *243*, 1.
(58) Bearpark, M. J.; Robb, M. A.; Schlegel, H. B. *Chem. Phys. Lett.* **1994**, *223*, 269.
(59) Andersson, K.; Malmqvist, P. A.; Roos, B. O. *J. Chem. Phys.* **1992**, *96*, 1218.
(60) Frisch, M. L.; *Gaussian 03, Revision C.02*; Gaussian Inc.: Wallingford, CT, 2004.
(61) Krogh, J. W.; *MOLCAS, version 6.2*; Lund University: Lund, 2003.
(62) Försberg, N.; Malmqvist, P.-Å *Chem. Phys. Lett.* **1997**, *274*, 196.
(63) Malmqvist, P.-Å.; Roos, B. O. *Chem. Phys. Lett.* **1989**, *155*, 189.
(64) Malmqvist, P. A.; Roos, B. O.; Serrano-Andres, L. *Chem. Phys. Lett.* **1998**, *288*, 299.
(65) Serrano-Andres, L.; Merchán, M.; Lindh, R. *J. Chem. Phys.* **2005**, *122*, 104107.
(66) Jortner, J.; Rice, S. A. *Adv. Photochem.* **1969**, *7*, 149.
(67) Siebrand, W. *J. Chem. Phys.* **1967**, *46*, 440.
(68) Siebrand, W. *J. Chem. Phys.* **1967**, *47*, 2411.

$$F(E) \approx e^{-4.5\cdot(E-0.51)} \quad \text{for} \quad E \geq 0.51\text{eV} \tag{2b}$$

Equations 2a and 2b are taken from ref 67−69.

If the process of interest is IC, then $V_{A,B} \geq 100$ cm^{-1} and the rate constant can be described by

$$k_{IC}(s^{-1}) = 10^{13}\cdot F \tag{3}$$

For an ISC process, $V_{A,B}$ is the spin−orbit coupling V_{so}, which can take values $0.1 < V_{so} < 50$ cm^{-1}, depending on the molecule and on the type of electronic states involved. Expressing V_{so} in cm^{-1}, the ISC rate constant of can be expressed by

$$k_{ISC}(s^{-1}) = 10^{9}V_{so}{}^{2}\cdot F \tag{4}$$

which accounts for ISC rates ranging from 10^7 to 10^{11} s^{-1}.

3. Results

3.1. Electronic Excited States Energies. 3.1.1. Vertical Excitation Energies. The CASSCF/6-31+G** optimized geometry of S_0, labeled Min S_0, is planar except for the slightly pyramidalized amino group: the two hydrogen atoms (linked to N_{10} in Scheme 1) are off the molecular plane by 21 and 19°, respectively, in striking agreement with the results obtained recently by the vibrational transition moment angles method.[71] Because the barrier height for the amino group inversion is only 0.01 eV,[71−73] the two amino hydrogens oscillate between the two minima, in agreement with the small inertial defect (−0.2) found in Ade microwave spectra.[72]

The size of the molecule and the presence of several N atoms with lone pairs lead to a rather complex electronic spectrum based on closely spaced nπ*, $\pi\pi$*, $\pi\sigma$*, and nσ* electronic states. The CASPT2 S_0-S_i excitation energies at the S_0 equilibrium geometry up to 6.5 eV are reported in Table 1. Transition energies and oscillator strengths are compared with the available experimental values.

As reported in previous studies,[1,2,5,20,74] the present energies of the three lowest excited states, ^{1}nπ*, ^1L_a, and ^1L_b are similar and range roughly from 4.4 eV (origin of ^{1}nπ* state) to ∼5.0 eV (vertical excitation of ^1L_a state) values. Because the calculated oscillator strengths of the ^{1}nπ* and ^1L_b absorption transitions are very small (≈10^{-2} and ≈10^{-3}, respectively), they depend markedly on the geometry chosen.[75] The oscillator strength for $S_0\rightarrow{}^1L_a$ excitation is higher, 0.22 at the CASSCF(12,9) level, and is responsible for most of the absorption in the spectral region at about 5 eV.

The computed vertical excitation energy to the ^1L_a state, 5.45 eV/5.20 eV with the (12,11)/(12,9) active spaces, is slightly higher than the experimental absorption maximum in vapor[1] (249 nm/4.98 eV) and in supersonic beam[17] (≈252 nm/4.92 eV).

Table 1. CASPT2//CASSCF/6-31+g**[a] Relative (ΔE) Energies and Oscillator Strength (f) for All the Relevant States Minima and for the Points Discussed in the Text along the ^1L_b and ^{1}nπ* Paths (Figure 1)

		CASPT2 (12,11)	CASPT2 (12,9)		exp. data	
structure	state	ΔE^b (eV)	ΔE^c (eV)	F	ΔE (eV)	F
Min S_0	ground st. (S_0)	0.00	0.00			
	^{1}nπ*	5.01	5.06	1.1×10^{-2}		
	^1L_b	5.07	5.07	1.8×10^{-3}		
	^1L_a	5.45	5.20	0.22	4.98[g]	0.24[g]
	$^1\pi\sigma_{N10H}$*	5.71				
	$^1\pi\sigma_{N9H}$*	5.86				
	^1B_b	6.36[d]	6.28	0.44	5.99[g]	∼0.48[g]
	^{1}nσ_{N9H}*	6.44[e]		8.5×10^{-2}[e]		
	^{1}nσ_{N9H}*	6.48[e]		0.11[e]		
Min L_b	S_0	−0.03	0.07			
	^1L_b	4.64	4.70	4.0×10^{-4}	4.47[f]	
	^{1}nπ*	4.73	4.89	9.5×10^{-3}		
	^1L_a	5.18	5.02	0.13		
	$^3\pi\pi$*	4.54				
	$^3\pi\pi$*	4.85				
Min nπ*	S_0	1.52	1.47			
	^{1}nπ*	4.44	4.30	2.9×10^{-3}	4.35[f]	
	^1L_b	5.85	6.05	1.0×10^{-2}		
	^1L_a	6.16	5.87	7.1×10^{-2}		
	^3L_a	4.34				
	$^3\pi\pi$*-^{3}nπ*	4.50				
CI S_0/nπ*	S_0	4.81	4.76			
	^{1}nπ*	4.90	4.68			
CI L_b/nπ*	^1L_b	4.64	4.70			
	^{1}nπ*	4.73	4.89			

[a] Nine roots state averaged wave function (SA-9). The (12,9) active space excludes the antibonding σ_{N9H}* and σ_{N10H}* orbitals. [b] The CASPT2 S_0 energy is −466.018695. [c] The CASPT2 S_0 energy is −466.018787. [d] SA-13, the CASPT2 S_0 energy is −466.017643 au and the CASSCF S_0 energy is −464.633587 au. [e] SA-13 energy values, these states are not included in the first nine roots; the CASPT2 S_0 energy is −466.018428 au and the CASSCF S_0 energy is −464.605239 au. [f] Jet-cooled Ade electronic spectra.[17] [g] Vapor phase absorption band maxima.[1] B_b osc. strength, according to Clark's spectrum,[1] is twice L_a as intense.

The lowest $^1\pi\sigma$* states, $\pi\sigma_{N10H}$* and $\pi\sigma_{N9H}$*, with the σ* orbital localized on the $N_{10}-H$ bond of the amino group and on the N_9-H bond of the azine group, are computed to be higher than the ^1L_a state by 0.26 and 0.41 eV, respectively. Their oscillator strength, f, is quite small (<10^{-3}) because their transitions to and from S_0 are forbidden in the planar geometry. These $^1\pi\sigma$* states have been proposed by several authors[24,46,47] as mediators in ^1L_a photodeactivation, by involving (aborted) hydrogen atom detachment.

At higher energies we find other absorbing electronic states: one, with the highest oscillator strength ($f = 0.44$, Table 1), is the ^1B_b $^1\pi\pi$* state, S_8, at 6.36/6.28 eV, that is associated with the most intense transition in the near-UV. These findings are quite in agreement with Clark's experimental data[1,76] that show an intense band at 5.99 eV for the 9Met-Ade in vapor phase.

3.1.2. ^1L_b and ^{1}nπ* Optimized Geometries. The CASPT2 excitation energies at the ^1L_b and ^{1}nπ* optimized structures (Min L_b and Min nπ*, respectively) are reported in Table 1, and the relevant structure parameters are given in Figure 1.

Optimization of ^1L_b leads to a larger hexagonal ring while leaving the molecule planar and leads to a decrease of the ^1L_b energy by 0.43 eV. The oscillator strength of the transition $S_0\rightarrow{}^1L_b$ remains small ($f \approx 10^{-3}$), but the polarization of $S_0-{}^1L_b$

(69) Birks, J. B. *Photophysics of Aromatic Molecules*; Wiley: London and Colchester, 1970.
(70) Michl, J.; Bonacic-Koutecky, V. *Electronic Aspects of Organic Photochemistry*; Wiley-Interscience: New York, 1990.
(71) Choi, M. Y.; Dong, F.; Han, S. W.; Miller, R. E. *J. Phys. Chem. A* **2008**, *112*, 7185.
(72) Brown, R. D.; Godfrey, P. D.; McNaughton, D.; Pierlot, A. P. *Chem. Phys. Lett.* **1989**, *156*, 61.
(73) McMullan, R. K.; Benci, P.; Craven, B. M. *Acta Crystallogr., Sect. B: Struct. Sci.* **1980**, *36*, 1424.
(74) Guéron, M.; Eisinger, J.; Shulman, R. G. *J. Chem. Phys.* **1967**, *17*, 4077.
(75) Conti, I.; Di Donato, E.; Negri, F.; Orlandi, G. *J. Phys. Chem. A* **2009**, published ASAP.
(76) Clark, L. B. *J. Chem. Phys.* **1990**, *94*, 2873.

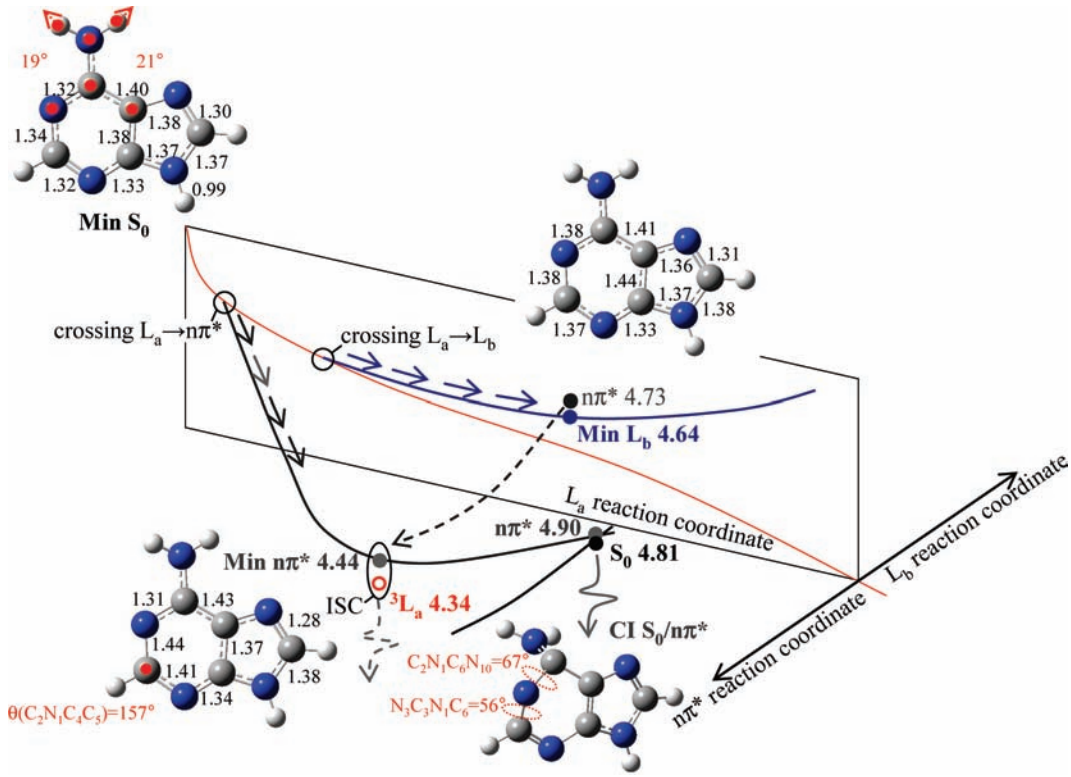

Figure 1. Schematical representation of nπ^* (gray line) and L_b (blue line) decay paths, which are crossed during the relaxation on the L_a MEP (red line) from the Franck−Condon region (Min S_0) to the crossing region with the ground state. Dashed gray line shows the way that connects Min L_b to Min nπ^*. Red circle represents the $^3\pi\pi^*$ (L_a type) triplet state almost isoenergetic with the nπ^* minimum (Min nπ^*). Energy values (eV) are reported in Table 2.

transition dipole moment (TDM) becomes almost parallel to the short molecular axis.[75]

The optimized geometry of the ^{1}nπ^* state is nonplanar because of the C_2 out-of-plane distortion by a ∼23° ($\theta(C_2N_1C_4C_5) = 157.5°$, Figure 1). The energy of the twin minima is 4.44 eV, that is, 0.54 eV lower than the energy of the vertical excitation. Roughly, this stabilization is due to the puckering deformation (0.34 eV) and the in-plane relaxation (0.2 eV). The $S_0-{}^1$nπ^* computed oscillator strength remains small, $\sim10^{-2}$, but its transition moment acquires also in-plane components.

The recent rotational band profile analysis of the C, D, and E bands by Lee et al.[25] gives the polarization of the transition dipole moments (TDMs) associated with the $S_0-{}^1$nπ^* and $S_0-{}^1L_b$ transitions and, thus, it allows to identify the higher excited states that are more strongly coupled with ^{1}nπ^* and ^1L_b.

In view of the shape of Ade, the *a*, *b*, and *c* inertial axes are the in-plane long, in-plane short, and out-of-plane axes, respectively. Our calculations at Min S_0 geometry indicate that the $S_0\rightarrow{}^1L_a$ and $S_0\rightarrow{}^1B_b$ TDMs are polarized *mainly* along the in-plane *a* (long) and *b* (short) inertial axis, respectively.

The rotational analysis presented in ref 25 indicates that the C band is polarized mostly along the *c* axis, while the D and E band are mainly polarized along the *b* (short) axis .

It follows that the C band must correspond to a vibronic state of ^{1}nπ^* that is based on a symmetric vibrational wave function with respect to the molecular plane.[20] The E band must represent a vibronic state of ^{1}nπ^*[20] that is based on an odd wave function of an out-of-plane vibration, which borrows the transition intensity mainly from the *b*-polarized $S_0-{}^1B_b$ transition. The D band, which is assigned to the 0−0 band of the $S_0\rightarrow{}^1L_b$ transition,[20] has a TDM oriented predominantly along the *b* (short) axis.[25] Therefore, both the E and the D bands, which are based on ^{1}nπ^* and ^1L_b electronic states, borrow their transition intensity mainly from the ^1B_b state rather than the energetically closer ^1L_a state. This fact suggests that the ^{1}nπ^*/^1L_a and ^1L_b/^1L_a interactions are weaker than the ^{1}nπ^*/^1B_b and ^1L_b/^1B_b couplings and, in turn, that the influence of ^1L_a on the spectroscopic as well as on the *photophysical* properties of the lower ^{1}nπ^* and ^1L_b electronic states tends to be weak.

3.2. Radiationless Decay of the ^{1}nπ^* and ^1L_b Excited States. 3.2.1. ^{1}nπ^* Decay Routes. Following vertical $S_0\rightarrow S_1(^1$n$\pi^*)$ excitation at the S_0 equilibrium structure, the molecule relaxes on the ^{1}nπ^* potential energy surface (PES) to Min nπ^* (Figure 1). At this geometry the $E(^1$n$\pi^*) - E(S_0)$ energy gap decreases to 2.92 eV, since $E(S_0)$ is 1.52 eV, and the $E(^1L_b) - E(^1$n$\pi^*)$ energy gap increases to 1.41 eV (see Table 1). Furthermore, the ^{1}nπ^* state is only slightly above the $T_1(^3\pi\pi^*)$ triplet: the $E(^1$n$\pi^*) - E(T_1(^3\pi\pi^*))$ energy gap is 0.10 eV (Table 1).

The lowest conical intersection between S_0 and ^{1}nπ^*, CI S_0/^{1}nπ^* (Figure 1), is found at about 4.86 eV, that is 0.42 eV above Min nπ^*, qualitatively similar to the previous results of 0.07[34] and 0.21 eV.[35] The path from Min nπ^* to the CI S_0/nπ^* involves mainly the torsion around the C_2-N_1 ($N_3C_2-N_1C_6 = 56°$) and N_1-C_6 bond leading to the bending of the amino group out of the molecular plane ($C_2N_1-C_6N_{10} = 67°$), as found in previous studies[11,13,31,33−35,38] and as shown in Figure 1.

The lowest ^1L_b/^{1}nπ^* CI is found at about 4.68 eV, about 0.24 eV above the ^{1}nπ^* energy minimum. This can provide a further decay path for ^{1}nπ^* provided that ^1L_b has an independent decay channel.

To summarize, four concurrent decay paths can be envisaged for ^{1}nπ^* (note that the two decays to S_0 are discussed separately

for operative reasons, even if they are part of the same process): (1) the $^1n\pi^* \rightarrow S_0$ IC occurring at Min $n\pi^*$, which may account for the low temperature decay of lowest vibronic levels of $^1n\pi^*$, namely, the A, C, and E bands observed in supersonic beams; (2) the $^1n\pi^* \rightarrow S_0$ IC process occurring at the $^1n\pi^*/S_0$ CI, which requires a proper amount of vibrational energy that is available exciting in a spectral region where most of the absorption is due to ^1L_a; (3) the $^1n\pi^* \rightarrow T_1$ ISC, which may account for the low and high temperature decay of $^1n\pi^*$; (4) the $^1n\pi^* \rightarrow {}^1L_b$ IC process occurring at the $^1n\pi^*/{}^1L_b$ CI, which will be discussed in the context of the ^1L_b decay because, as we shall see, this CI is apt to favor the opposite $^1L_b \rightarrow {}^1n\pi^*$ rather than the $^1n\pi^* \rightarrow {}^1L_b$ IC process.

Because the $S_0 \rightarrow {}^1n\pi^*$ absorption coefficient is negligible, these processes might only account for the τ_2 decay observed exciting ^1L_a.

The rate of the $^1n\pi^* \rightarrow T_1(\pi\pi^*)$ ISC process is given by eq 4 and depends on the square of the spin−orbit coupling V_{so} and on the FC factor F. Our CASSCF calculations led to $V_{so} = 11$ cm^{-1}, a value similar to the result (4 cm^{-1}) obtained by Blancafort.[35] Because the F factor computed by eq 2a is 0.3, we estimate by eq 4 $k(^1n\pi^* \rightarrow T_1(\pi\pi^*)) \approx 0.4 \times 10^{11}$ s^{-1}, which would correspond to a lifetime of 25 ps. The rate of the vertical $^1n\pi^* \rightarrow S_0$ decay route can be estimated by eq 3 and requires the evaluation of the F factor according to eqs 2a and 2b. We assume that S_0 energy at the Min $n\pi^*$ (1.52 eV) is absorbed by the C_2 puckering coordinate and consider the remaining energy gap of 2.92 eV according to eq 3. In this way, we get $F \approx 1.3 \times 10^{-6}$ (2×10^{-6}) and this leads to the rate $k(^1n\pi^* \rightarrow S_0) = 2 \times 10^7$ s^{-1}.

Thus, it appears that the most efficient decay route of the vibrationless $^1n\pi^*$ state is the $S_1(n\pi^*) \rightarrow T_1(\pi\pi^*)$ ISC. It is worth noting that this estimated lifetime of $S_1(n\pi^*)$, 25 ps, is compatible with the experimental lifetimes (≈50 ps) of the vibronic bands C and E.[24,25]

The $^1n\pi^* \rightarrow S_0$ IC process can occur at the $^1n\pi^*/S_0$ CI that we computed at an energy 0.42 eV above Min $n\pi^*$, to be compared with the value of 0.21 eV found by Blancafort.[35] The structure of this CI is shown in Figure 1. The $^1n\pi^* \rightarrow S_0$ IC process at the $^1n\pi^*/S_0$ CI requires a proper amount of vibrational energy in an isolated-molecule system, larger than the E(CI $S_0/{}^1n\pi^*$) − E(Min $n\pi^*$) energy gap. In an equilibrated system it requires a substantial thermal activation. Because we wish to discuss the data obtained in supersonic beam, we calculated the rates of the $^1n\pi^* \rightarrow S_0$ IC process at the $^1n\pi^*/S_0$ CI by the RRKM approach[77,78] for several values of vibrational energy contents (for molecules having vibrational frequencies ≥300 cm^{-1}, it can be assumed that the vibrational thermalization occurs within 0.1 ps; thus, the RRKM calculations to evaluate decay times ≥1 ps should be reliable). The values chosen are the difference between the excitation energy hν and the energy of the lowest observed (A) band,[21] neglecting the vibrational energy compatible with the beam vibrational temperature <50 K. In particular, we consider the photon energies corresponding to three excitation wavelengths used in the Ade photophysical studies: 272, 263, 250 nm.[31,32] The two sets of vibrational frequencies, which are reported in the SI in Table S6, were computed at Min $n\pi^*$ and at a geometry very close to the $^1n\pi^*/S_0$ CI: the latter set contained one imaginary frequency. Two values of barrier energies (E_b) were chosen: 0.42 and 0.21 eV, corresponding to the $^1n\pi^*/S_0$ CI energies of this work and of ref 35, respectively.

Table 2. Evaluation of $^1n\pi^*$ State Lifetimes (τ) at Different Excitation Energies (λ_{exc}) and Energy Barriers (E_b) by the RRKM[77,78] Approach

	λ_{exc} = 272 nm	λ_{exc} = 263 nm	λ_{exc} = 250 nm
E_b = 0.42 eV[a]	∞	∞	10 ns
E_b = 0.21 eV[b]	∞	103 ps	15 ps

[a] CASPT2//CASSCF/6-31+g** calculated barrier, see Min $n\pi^*$ and CI $S_0/n\pi^*$ energy values in Table 1. [b] Ref 35

The resulting $^1n\pi^*$ lifetimes (τ) are shown in Table 2. We note that these lifetimes (a) are longer than the observed Ade τ_2 (1 ps) and (b) strongly depend on the excitation energy, while the experimental τ_2 varies roughly only from 1 to 2 ps.[31,32] This indicates that the $^1n\pi^* \rightarrow S_0$ process at the $^1n\pi^*/S_0$ CI cannot be responsible of the τ_2 lifetime measured in supersonic beams.

Thus, we conclude that the decay of $^1n\pi^*$ is dominated by $^1n\pi^* \rightarrow T_1(\pi\pi^*)$ ISC process.

3.2.2. ^1L_b Decay Routes. After the vertical $S_0 \rightarrow {}^1L_b$ excitation (at 5.07 eV), the Ade molecule has a vibrational energy of 0.43 eV with respect to the Min L_b energy of 4.64 eV (Table 1). With this available energy, no $^1L_b/S_0$ CI was intercepted. Furthermore, no $^1L_b/S_0$ CI was identified at a reasonable energy above the ^1L_b minimum.

As specified in Table 1, we found a $^1L_b/{}^1n\pi^*$ CI about 0.05 eV above the ^1L_b minimum, comparable with the value of 0.14 eV reported by Merchan.[33] This indicates that a fast $^1L_b \rightarrow {}^1n\pi^*$ conversion can take place.

We have looked without success for triplet states with an appreciable $<{}^1L_b(\pi\pi^*)/H_{so}/{}^3n\pi^*>$ spin−orbit coupling (V_{so}) and at energies close to $E(^1L_b)$. The closest triplet state, $T_2(\pi\pi^*)$, has a small $<{}^1L_b/H_{so}/T_2>$ coupling (<0.1 cm^{-1}). This suggests that the ISC processes from ^1L_b to lower energy triplet states are not efficient. Therefore, fast decay channels leading to S_0 via triplet states apparently are not available for ^1L_b.

In conclusion, the main ^1L_b decay channel involves the crossing to $^1n\pi^*$ and its overall decay rate should be very similar to that of $^1n\pi^*$ state: this agrees with the observed similarity of the lifetimes of the $^1n\pi^*$ and ^1L_b states (ca. 50 ps) as estimated by the line width of the C, D, and E bands in the R2PI spectrum in supersonic beam.[24,25]

3.3. Radiationless Decay of the ^1L_a Excited State. 3.3.1. ^1L_a Decay Paths. The decay paths of the ^1L_a state are the most interesting because this state absorbs practically all the light in the spectral region 270−240 nm, where the first strong band in the absorption of Ade is observed. Exciting λ <270 nm, two lifetimes were observed by several authors, 0.07−0.1 ps and 1−1.1 ps,[16,28−31] both much shorter than the lifetimes that may be attributed to the ^1L_b and $^1n\pi^*$ states, as discussed (vide supra). At the same time, the diffuse band appearing in the R2PI spectrum is completely absent in the fluorescence excitation spectrum,[17] which ends after the E band: this indicates an abrupt increase of the nonradiative decay rate as soon as the exciting beam frequency reaches the ^1L_a state.

In Table 3 and Figure 2, we present the MEP on the ^1L_a PES from the Min S_0 geometry to the lowest energy $S_0/{}^1L_a$ CIs, together with the energy profiles of the lowest excited states, in particular $^1n\pi^*$, ^1L_b, and $\pi\sigma^*$. As explained in the Computational Methods section, we have performed two parallel calculations by the CASPT2//CASSCF(12,9)-SA-9 and the MSPT2//CASSCF(12,11)-SA-9 based on an extended

(77) Robinson, P. J.; Holbrook, K. A. *Unimolecular Reactions*; Wiley-Interscience: New York, 1972.
(78) Marginean, I. http://phd.marginean.net/rrkm.html.

Table 3. CASPT2//CASSCF/6-31+g** and MSPT2//CASSCF/6-31+g** Relative (ΔE) Energies for Relevant Points along the L_a Path[a]

		CASPT2			MSPT2			
		(12,11)	(12,9)		(12,11)	dihedral angle (°)		
structure	state	ΔE^b (eV)	ΔE^c (eV)	f	ΔE^d (eV)	θ^e	ϕ^e	$\theta-\phi$
Min S_0	S_0	0.00	0.00		0.00	180	180	0
	S_1 ($n\pi^*$)	5.01	5.06	1.1×10^{-2}	5.03			
	S_2 (L_b)	5.07	5.07	1.8×10^{-3}	5.14			
	S_3 (L_a)	5.45	5.20	0.22	5.58			
	S_5 ($\pi\sigma_{NH2}^*$)	5.71			5.76			
	S_6 ($\pi\sigma_{N9H}^*$)	5.86			5.93			
IRC_1	S_1 (L_b)	4.91	4.78	2.1×10^{-3}	5.16	180	180	0
	S_2 (L_a)	5.13	4.72	0.236	4.79			
	S_3 ($n\pi^*$)	5.39	5.26	4.7×10^{-3}	5.42			
	S_4 ($\pi\sigma_{NH2}^*$)	5.55			5.52			
	S_5 ($\pi\sigma_{N9H}^*$)	5.55			5.91			
IRC_2	S_1 (L_b)	4.93	4.81	4.7×10^{-3}	5.24	178	178	0
	S_2 (L_a)	5.00	4.73	0.22	4.79			
	S_3 ($\pi\sigma_{N9H}^*$)	5.50			5.56			
	S_4 ($n\pi^*$)	5.50	5.39	2.9×10^{-3}	5.50			
	S_5 ($\pi\sigma_{NH2}^*$)	5.75			5.94			
IRC_3	S_1 (L_b)	4.93	4.82	5.8×10^{-3}	5.27	174	175	−1
	S_3 (L_a)	4.94	4.74	0.21	4.77			
	S_5 ($\pi\sigma_{N9H}^*$)	5.49			5.57			
	S_2 ($n\pi^*$)	5.52	5.41	5.2×10^{-3}	5.52			
	S_4 ($\pi\sigma_{NH2}^*$)	5.88			5.98			
IRC_4	S_1 (L_b)	4.93	4.83	6.9×10^{-3}	5.27	171	171	0
	S_2 (L_a)	4.99	4.76	0.20	4.71			
	S_3 ($\pi\sigma_{NH2}^*$)	5.49			5.60			
	S_4 ($n\pi^*$)	5.53	5.43	8.5×10^{-3}	5.54			
	S_5 ($\pi\sigma_{N9H}^*$)	5.87			6.01			
IRC_5	S_1 (L_b)	4.93	4.84	8.2×10^{-3}	5.27	167	168	−1
	S_2 (L_a)	5.07	4.78	0.18	4.67			
	S_3 ($\pi\sigma_{NH2}^*$)	5.41	0.00		5.64			
	S_4 ($n\pi^*$)	5.55	5.45	1.2×10^{-2}	5.57			
	S_5 ($\pi\sigma_{N9H}^*$)	5.89			6.03			
IRC_6	S_1 (L_b)	4.94	4.86	9.5×10^{-3}	5.27	164	164	0
	S_2 (L_a)	5.21	4.79	0.16	4.62			
	S_3 ($\pi\sigma_{NH2}^*$)	5.23			5.62			
	S_4 ($n\pi^*$)	5.58	5.49	1.4×10^{-2}	5.70			
	S_5 ($\pi\sigma_{N9H}^*$)	6.07			6.15			
IRC_7	S_1 (L_b)	4.96	4.89	1.1×10^{-2}	5.27	161	161	0
	S_2 (L_a)	5.05	4.80	0.14	4.61			
	S_3 ($\pi\sigma_{NH2}^*$)	5.50			5.81			
	S_4 ($n\pi^*$)	5.62	5.53	1.5×10^{-2}	5.68			
	S_5 ($\pi\sigma_{N9H}^*$)	6.14			6.24			
HPM	S_1 (L_a)	4.62	4.56	6.1×10^{-2}		146	139	7
	S_2 ($n\pi^*$)	5.37	5.28	2.1×10^{-3}				
	S_3 (L_b)	5.77	5.61	3.2×10^{-3}				
IRC_8	S_0	2.10	2.07			143	134	9
	S_1 (L_a)	4.54	4.40	5.8×10^{-2}				
IRC_9	S_0	2.40	2.32			140	129	11
	S_1 (L_a)	4.45	4.30	4.0×10^{-2}				
IRC_{10}	S_0	2.84	2.71			138	124	14
	S_1 (L_a)	4.41	4.27	3.8×10^{-2}				
IRC_{11}	S_0	3.19	3.05			137	118	19
	S_1 (L_a)	4.25	4.11	2.7×10^{-2}				
CI S_0/L_a	S_1 (L_a)	4.26	3.80			134	108	26
	S_0	3.79	3.90					

[a] Nine roots state averaged wave function (SA-9). The (12,9) active space excludes the antibonding σ_{N9H}^* and σ_{N10H}^* orbitals . [b] ΔE value refer to CASPT2 −466.018695 S_0 energy value. [c] ΔE value refer to CASPT2 −466.018787 S_0 energy value. [d] ΔE value refer to multistate CASPT2 −466.02136 S_0 energy value. [e] θ and ϕ are the $C_2N_1C_4C_5$ and $H_2N_1C_4C_5$ dihedral angles, respectively.

active space (including also σ_{N9H}^* or σ_{N10H}^* virtual orbitals localized on the azine N_9-H bond (σ_{N9H}^*) or on one $N_{10}-H$ bond of the amino group (σ_{N10H}^*), respectively (see Table 3 and Figure 2).

The photoinduced motion described by the two approaches is the same. The ^1L_a MEP, beginning at the vertically excited ^1L_a, enters (IRC_1, Figure 2) into an energy *plateau* characterized by changes of planar coordinates, in particular, of the CC and CN bonds lengths, with a stabilization energy of ≈0.4 eV (see Table 3). Note that the accuracy of the ^1L_a *relative energy* profile is confirmed by subtracting the calculated ^1L_a planar relaxation energy (0.4 eV) from the experimental ^1L_a absorption maximum (4.98 eV):[1] this leads to predict the ^1L_a energy plateau at ≈4.58 eV. Remarkably, this corresponds nicely to the lower limit of the diffuse absorption band observed at ≈4.6 eV in the Ade supersonic beam R2PI spectrum.[25] At this stage, ^1L_a state has become lower than any other excited state. Then the ^1L_a MEP (red line, Figure 2) proceeds to nonplanar distortions, associated with a mild energy decrease, which correspond to an out-of-plane C_2 ring puckering ($\theta(C_2N_1C_4C_5)$) involving mainly the pyramidalization of the carbon atom (Figure 2). These nonplanar distortions lead into a *dynamical trap* (around IRC_7), where the MEP wanders for a while into a wide and flat energy region before finding an exit path (HPM), characterized by the activation of a previously silent coordinate, which corresponds to the out-of-plane motion of the H_2 hydrogen atom ($\theta-\phi$, Figure 2). Once it is out of the plateau, the MEP shows a rapid energy drop leading to the S_0/L_a CI, located at about 4 eV. *We believe that the MEP summarized above is a rough representation of the molecular trajectories after the excitation to ^1L_a, and that the plateau is a feature of the ^1L_a PES that acts as a dynamical barrier that slows the decay toward the S_0/L_a CI and gives origin to the biexponential decay kinetics.* In other words, we attribute both the observed exponential decays to the ^1L_a state: the faster process represents the initial relaxation after excitation, the slower process is associated with the exit from the plateau.

This picture is indirectly supported by the findings of the previous sections, which showed that both ^1L_b and $^1n\pi^*$ decays with a lifetime longer than the τ_2 time constant (1 ps) observed in the ^1L_a decay. This implies that, despite ^1L_a crosses $^1n\pi^*$ and ^1L_b at the beginning of the MEP (see Figure 2 and Table 3), the $^1L_a \rightarrow {}^1n\pi^*$ and $^1L_a \rightarrow {}^1L_b$ IC processes are not efficient enough to compete with the direct decay on ^1L_a. This implication is consistent with both the small coupling between ^1L_a and $^1n\pi^*$ or ^1L_b (see section 3.1.2), suggested by the rotational analysis of the vibrational bands in R2PI spectra[25] and the notion that the $^1L_a \rightarrow {}^1L_b/{}^1n\pi^*$ transitions are hindered by the required significant change of trajectory direction (the molecular deformations occurring during the ^1L_a decay path are different than those following the $^1n\pi^*$ and ^1L_b decay paths). Finally, as proved by the RRKM calculations presented above in section 3.2.1, the time constant (τ_2) should depend markedly on the excitation energy, if it were associated with the $^1n\pi^*$ or ^1L_b decay. However, this τ_2 dependence is not observed.[31,32]

This conclusion is in agreement with other authors[11,13,14,33−35,38,55] and, conversely, tends to rule out the decay via the ^1L_b and $^1n\pi^*$ states proposed in earlier studies.[11,13,15,33−36,38,56]

This picture, leading to a lonely decay of ^1L_a directly to S_0, is supported by the results of TRPES measures in supersonic beams[16,28−30] and by the recent time-resolved fluorescence spectra in aqueous solutions.[44] The comparison of the present theoretical results with these recent experimental data, which will be discussed below, is quite illuminating.

3.3.2. Time Resolved Photoelectron Spectra (TRPES). The TRPES following Ade ^1L_a excitation, which were measured by Stolow and co-workers,[16,28−30] extend up to 10.5 eV and have

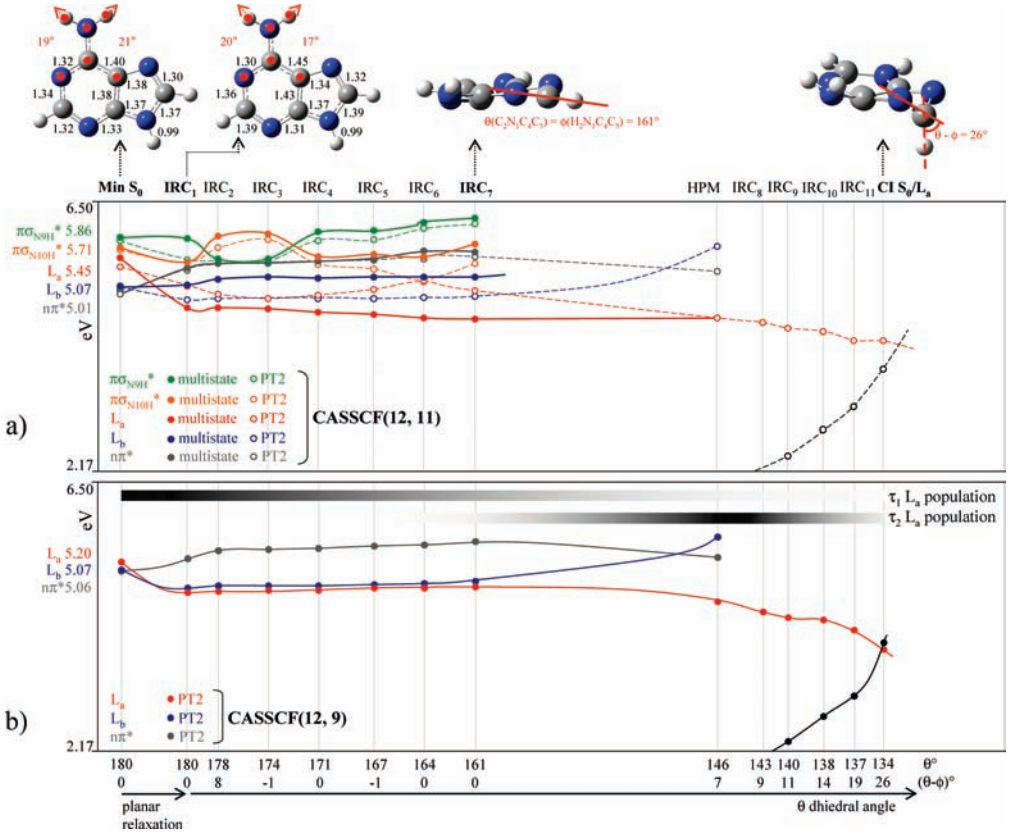

Figure 2. Potential energy surface profiles along the L_a minimum energy path (MEP, red line). (a) CASPT2 (dashed lines) and multistate-CASPT2 (continuous lines) energy values (eV), calculated on a CAS(12,11)/6-31+g** wave function. (b) CASPT2/6-31+g** L_a, L_b, and nπ* PES profiles, CASSCF active space (12,9), where σ* orbitals are omitted. Energy values are in Table 2. θ and ϕ dihedral angles correspond to $C_2N_1C_4C_5$ and $H_2N_1C_4C_5$, respectively. They ensure the out of plane movement of C_2 and H_2.

been resolved in two spectra decaying with 0.07−0.1 and 1.1 ps time constants,[16] respectively. The shorter lived transient shows bands in the region from 8.5 to 10.2 eV,[16] while the longer lived spectrum shows electron energies in the range 9.5−10.5 eV.[16] Similar experiments were performed by Canuel et al. and Ritze et al.[12,45] with analogous results.

The transient TRPES are built on the ionization potentials (IPs) of the occupied MOs that are involved in the electronic configurations of the transient electronic states that are produced during the decay. Obviously, they are modeled also by the FC structure of the probing (ionizing) transition.

To identify the excited electronic state responsible of a given TRPES response, we compare the transient TRPES with the computed IPs. The latter were evaluated by employing correlated (CASPT2//CASSCF) energies. Specifically, taking as a reference the energy of the neutral Ade at the initial Min S_0 geometry, IPs of *short-lived* or of *structurally stable* excited states are estimated as the energies of the ions in their ground and excited states at the same Min S_0 geometry. The IPs for transient states undergoing geometry changes during their lifetime are obtained computing also the ion energies at modified geometries. Thus, for the longer lived ^{1}nπ* and ^1L_b states we have evaluated also the IPs at the Min nπ* and Min L_b structures. For the short-lived but strongly deforming ^1L_a state, we have computed the IPs also at a number of geometries along the ^1L_a decay path. The main results are reported in Table 4.

At the S_0 geometry, the IPs derived for the cation lowest excited states and corresponding to the highest MOs energies are 8.49 (π_H), 9.24 (n_1), 9.65 (π_{H-1}), 10.52 (π_{H-2}), and 10.71 (n_2). Combining this information with the CASSCF(12,11) wave functions of the lowest ^1L_a, ^{1}nπ*, and ^1L_b excited states,

Table 4. CASPT2//CASSCF[a] Ionization Energy (IP) Values and CASSCF[b] Singlet Wave Functions[c]

structure	state	singlets wave functions: transition	Coeff.	half-filled orbital	calcd IP (eV)
Min S_0	L_a	$\pi_H \rightarrow \pi_L$*	0.71	π_H	8.49
		$\pi_{H-1} \rightarrow \pi_{L+1}$*	0.33	π_{H-1}	9.65
		$N_1 \rightarrow \sigma_{N10H}$*	0.29	n_1	9.24
				π_{H-2}	10.52
				n_2	10.71
				π_{H-3}	12.48
IRC_7	L_a	$\pi_H \rightarrow \pi_L$*	0.67	π_H	8.57
		$\pi_H \rightarrow \sigma_{N10H}$*	0.42		
		$\pi_{H-1} \rightarrow \pi_L$*	0.26	π_{H-1}	9.98
HPM	L_a	$\pi_H \rightarrow \pi_L$*	0.78		
		$\pi_H \rightarrow \sigma_{N10H}$*		π_H	9.35
		$\pi_{H-1} \rightarrow \pi_L$*		π_{H-1}	10.85
IRC_{11}	L_a	$\pi_H \rightarrow \pi_L$*	0.71	π_H	10.18
Min L_b	L_b	$\pi_{H-1} \rightarrow \pi_L$*	0.66	π_{H-1}	9.57
		$\pi_H \rightarrow \pi_{L+1}$*	0.58	π_H	8.36
Min nπ*	nπ*	$n_1 \rightarrow \pi_L$	0.79	n_1	10.02
		$\pi_H \rightarrow \pi_L$*	0.42	π_H	9.53
CI S_0/nπ*	nπ*	$n_1 \rightarrow \pi_L$	0.82	n_1	11.40

[a] CASSCF(11,11)/6-31+g**-SA-9 wave function has been employed. [b] Singlet CASSCF(12,11)/6-31+g** wave functions are reported. [c] π_H orbital is the bonding orbital mainly involved in ^1L_a electronic state excitation; π_{H-1} together with π_H in ^1L_b state. n_1 is a linear combination of "n" type orbital with opposite sign on N_1 and N_3 nitrogen atoms, n_2 with the same sign; π_{H-2} and π_{H-3} are π orbitals at lower energies.

$$\Psi(^1L_a) \approx [0.71(\pi_H \rightarrow \pi_L^*) + 0.29(n_1 \rightarrow \sigma_{N10H}^*) + 0.33(\pi_{H-1} \rightarrow \pi_{L+1}^*)]$$

$$\Psi(^1L_b) \approx [0.62(\pi_H \rightarrow \pi_{L+1}^*) + 0.62(\pi_{H-1} \rightarrow \pi_L^*)]$$

$$\Psi(^1n\pi^*) \approx [0.84(n_1 \rightarrow \pi_L^*)]$$

we easily derive which orbital IP signatures characterize the transient TRPES spectrum of a specific electronic state. The CASSCF(12,11) wave functions indicate that the ^1L_a TRPES should include the contribution of three IPs, namely, at 8.5(π_H), 9.2(n_1), and 9.6($_{H-1}$) eV, dressed by their FC structures. Correspondingly, the ^1L_b and $^1n\pi^*$ TRPES include two IPs, namely, at 8.5 and 9.6 eV, and one IP at 9.2 eV, respectively. Thus, keeping in mind the existence of the FC envelop, we expect from these data that the ^1L_a and ^1L_b TRPES extend from 8.5 to 9.6 eV and above taking into account the FC structure. For the same reason the $^1n\pi^*$ TRPES should extend above 9.2 eV. This would associate both the ^1L_a and ^1L_b states with the short-lived (0.1 ps) transient and $^1n\pi^*$ with the longer lived (1 ps) species. Because ^1L_b can be ruled out, for the low $S_0 \rightarrow {}^1L_b$ transition moment, as the parent of the short-lived (0.1 ps) transient, we would confirm at this stage the usual assignment.[16,28−30] Note that using the IPs computed at Min $n\pi^*$and Min L_b structures leads to the same conclusions.

To pursue the proposal that ^1L_a is responsible also of the 1 ps transient (see section 3.3.1), we computed also the IPs at geometries along the ^1L_a MEP.

We can see that, moving from Min S_0 to IRC_7 (the *dynamical trap* region), HPM and IRC_{11} geometries, the π_H IP moves from 8.5 eV to 8.57, 9.35, and 10.18 eV, respectively. Thus, Ade IPs at the HPM geometry are compatible with the observed longer lived TRPES spectrum.[16] This supports the theoretical results presented above in section 3.3.1. Furthermore, the change of IPs during the motion on the MEP toward the plateau can generate a multiplicity of spectral envelopes that adds broadness to the Ade TRPES spectrum. In conclusion, it appears that the decay path on the ^1L_a MEP suffices to account for the two components of the TRPES spectra.

3.3.3. Time-Resolved Fluorescence. Recently, Phillips and coworkers[44] have measured time-resolved fluorescence spectra of adenosine in aqueous solutions. In water solutions, like EG/water, the $^1n\pi^*$ state has a higher energy than in the gas phase[12,13,39,40] and is not the lowest singlet any more.

The decay kinetics after exciting at 267 nm was found biexponential,[44] with time constants $\tau_1 = 0.15$ ps and $\tau_2 = 0.45$ ps, and the two fluorescence spectral components were determined. These time parameters are reminiscent of the lifetimes, 0.1 and 1 ps, of the isolated Ade[16,28−32] and very similar to the lifetimes measured in Ade$(H_2O)_n$ water complexes.[45]

The measured radiative rate constants[44] of the two transient species are $k_1 = 2.32 \times 10^8$ and $k_2 = 0.57 \times 10^8$ s^{-1}, respectively. The short-lived fluorescence spectrum shows a maximum at 310 nm, is comprised between 285 and 400 nm, and is reminiscent of the fluorescence spectrum recorded at 77 K in EG/water.[44] The longer-lived spectrum is more broadened, from 305 to 550 nm, with the maximum at about 392 nm.

From the two measured radiative rate constants we can derive the oscillator strengths of the two transitions, f_1 and f_2, by use of the relation[69]

$$f = 1.5 \cdot k(s^{-1}) \cdot (c/\nu)^2$$

Table 5. CASPT2//CASSCF[a] Energy Gap $\lambda(E_{exc} - E_{S0})$ and Oscillator Strength (f) Value between the Excited State and the Ground States[b]

Structure	*State*	*Calc. data*		*Exp. Data*	
		$(\lambda_{exc}-\lambda_{S0})$ *(nm)*	f	*Spectrum E gap (nm)*	
				τ_1	τ_2
Min S_0	L_a	238	$2.2x10^{-1}$		
IRC_1	L_a	268	$2.4x10^{-1}$		
IRC_2	L_a	277	$2.2x10^{-1}$	285	
IRC_3	L_a	278	$2.1x10^{-1}$	.	
IRC_4	L_a	280	$2.0x10^{-1}$	.	
IRC_5	L_a	283	$1.8x10^{-1}$	τ_1 .	
IRC_6	L_a	289	$1.6x10^{-1}$	.	
IRC_7	L_a	297	$1.4x10^{-1}$	.	305
HPM	L_a	442	$6.1x10^{-2}$	400	τ_2 .
IRC_8	L_a	533	$5.8x10^{-2}$		.
IRC_9	L_a	624	$4.0x10^{-2}$		550
IRC_{10}	L_a	794	$3.8x10^{-2}$		
IRC_{11}	L_a	1162	$2.7x10^{-2}$		
Min L_b	L_b	268	$0.4x10^{-3}$		
Min $n\pi^*$	$n\pi^*$	438	$2.9x10^{-3}$		

[a] CASSCF(12,9)/6-31+g**-SA-9 wave function has been employed. [b] At a number of geometries along the L_a MEP and on $n\pi^*$ and L_b minima.

where $\nu(s^{-1})$ is the average transition (spectral) frequency and c is the light velocity (cm s^{-1}).

Estimating from the transient spectra[44] $(\nu_1/c) = 32250$ cm^{-1} and $(\nu_2/c) = 25500$ cm^{-1}, and using the above k_1 and k_2 values, we get $f_1 = 0.33$ and $f_2 = 0.13$ for the faster and the slower decay, respectively.

We note that the value of f_1 corresponds qualitatively to the ^1L_a oscillator strength computed at the ground state geometry (0.22, see Table 5), and f_2 is similar to the ^1L_a oscillator strength in the region of the IRC_7 and HPM geometries (0.14−0.06, see Table 5). On the contrary, the f_2 value is much larger than the oscillator strength calculated for the $S_0 \rightarrow {}^1n\pi^*$ (≈0.003) and $S_0 \rightarrow {}^1L_b$ (<0.001) transitions (see Table 5), ruling out the association of both emissions with the $^1n\pi^*$ and ^1L_b states. In addition, the maxima of the two fluorescence spectral components, associated with the short (τ_1) and the long (τ_2) lifetimes, match roughly the L_a-S_0 energy gaps in the initial part (IRC_1) and the plateau region (IRC_7) of the L_a MEP, respectively (as shown in Table 5).

Thus, according to the time-resolved fluorescence spectra[44] of adenosine in aqueous solution, the slower (≈ 1 ps) decay of Ade cannot be due to the ^1L_b or the $^1n\pi^*$state, but, rather, it reflects the decay of ^1L_a *at structures corresponding to the plateau region that are kinetically distinct from the relaxing vertically excited structure*. This conclusion agrees with the results of the TRPES[16,28,30] discussed above and with our calculations.

3.4. Transition from ^1L_a to$^1\pi\sigma_{NH}^*$ Excited States: N−H Photocleavage. Several authors, in particular, Sobolewski and Domcke, have highlighted the dissociative character with respect to N−H bond of the $^1\pi\sigma_{N9H}^*$ ($^1\pi\sigma_{N10H}^*$) states[9−16] and proposed that these states would play an important role in the N−H bond photocleavage. Here, we wish to re-examine this process by considering the $^1L_a \rightarrow {}^1\pi\sigma_{N9H}^*$ ($^1\pi\sigma_{N10H}^* \rightarrow S_0$ IC, with aim to determine the energies at which it may be activated.

According to our calculations (vide supra), the ^1L_a MEP does not intercept the energy curve of any $^1\pi\sigma^*$ state and remains below these states all the way from the vertical excitation to the CI S_0/L_a geometry. The smallest $E(^1\pi\sigma_{N10H}^*) - E(^1L_a)$ and $E(^1\pi\sigma_{N9H}^*) - E(^1L_a)$ energy gaps are found at the ground state

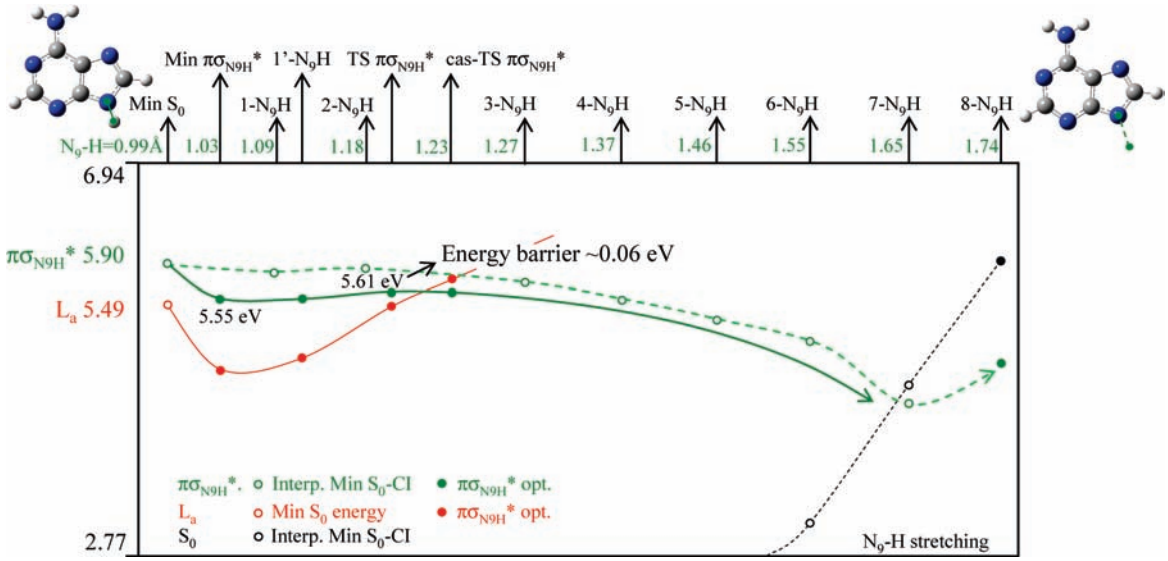

Figure 3. $\pi\sigma_{N9H}$* reaction paths (green line) along the N_9-H bond length coordinate. Note that the diagram scale is larger for N_9-H bond length lower than 1.27 Å. Dashed lines (and empty circles) belong to simple $\pi\sigma_{N9H}$* geometry interpolation between FC region (Min S_0 structure) and 8-N_9H structure (belonging to optimized CASSCF crossing region). Continuous lines (and filled circles) belong to optimized structures on $\pi\sigma_{N9H}$* along the N_9-H stretching coordinate (coordinate-driven MEP). Energy values are reported in Table 5. The cas-TS $\pi\sigma_{N9H}$* point does not coincide with the PT2 barrier (0.06 eV, TS $\pi\sigma_{N9H}$*): this confirms the flatness of that region (see Table 5 captions).

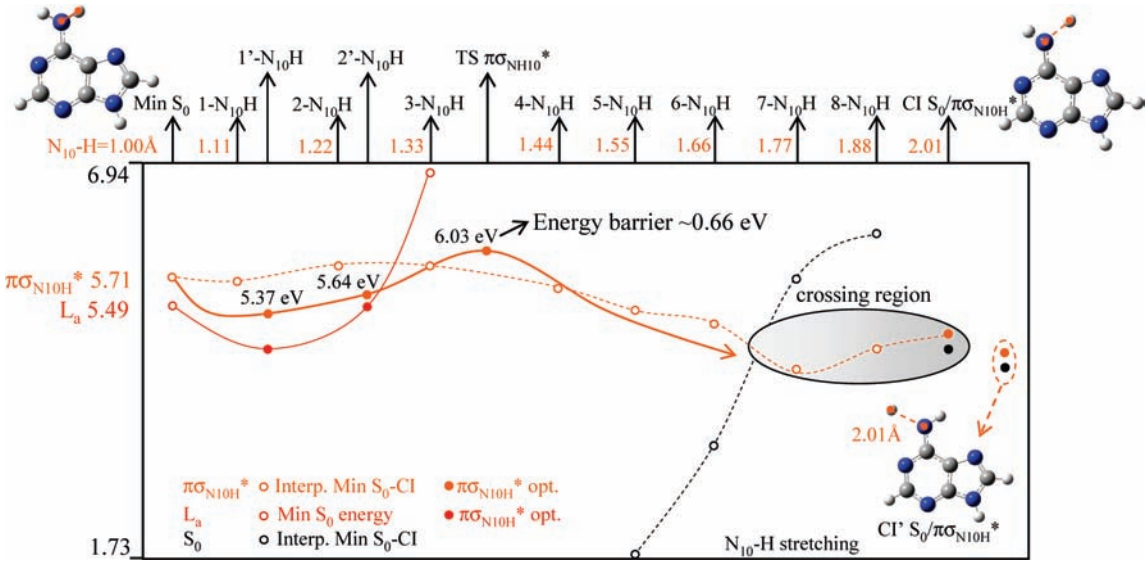

Figure 4. $\pi\sigma_{N10H}$* reaction paths (orange line) along the $N_{10}-H$ bond length coordinate. Dashed lines (and empty circles) belong to simple $\pi\sigma_{N10H}$* geometry interpolation between FC region (Min S_0 structure) and the CI $S_0/\pi\sigma_{N10H}$* structure (belonging to optimized CASSCF crossing region). Continuous lines (and filled circles) belong to optimized structures on $\pi\sigma_{N10H}$* along the $N_{10}-H$ stretching coordinate (coordinate-driven MEP). Energy points are reported in Table 5.

equilibrium geometry (Figure 2a), where they are 0.22 and 0.41 eV, respectively (see Table S7 in SI). For comparison, the smallest calculated vertical $E(^1\pi\sigma^*) - E(^1L_a)$ energy gap found in the literature is ~0.4 eV.[13]

We have computed the N_9-H and the $N_{10}-H$ stretching potential energy curves in the $^1\pi\sigma_{N10H}$* and $^1\pi\sigma_{N9H}$* states, respectively, by optimizing at some chosen N−H bond lengths all the remaining molecular coordinates. These optimized energy curves are shown in Figures 3 and 4, together with the corresponding ^1L_a energy profile. Both $^1\pi\sigma^*$ energy curves are highly unharmonic and, except for the initial relaxation out of the FC structure, are much flatter than the corresponding ^1L_a energy profile. Furthermore, they reveal a barrier along the N−H bond cleavage that is small (0.06 eV) for $^1\pi\sigma_{N9H}$* but is much higher (0.66 eV) for $^1\pi\sigma_{N10H}$*. Energy values are given in Table S7 of SI.

As a consequence, the zero point energy ($h\nu_{NH}/2$) of the N−H stretch vibration is quite different in the two states:[12] it is estimated ~0.2 eV in ^1L_a, but it is much smaller (almost negligible) in the $^1\pi\sigma^*$ states and, in particular, $\pi\sigma_{N9H}$* (see Table S8 and Scheme S1 in SI). Furthermore, the $^1\pi\sigma^*$ and ^1L_a energy curves must cross and, in fact, the crossing occurs at N−H lengths (1.18 and 1.22 Å for $\pi\sigma_{N9H}$* and $^1\pi\sigma_{N10H}$*, respectively) that are slightly longer than equilibrium distances.

At these N−H bond lengths, the NH stretch FC factors for the $^1L_a \rightarrow {}^1\pi\sigma^*$ radiationless transition are maximized and, accordingly, the rate of the $^1L_a \rightarrow {}^1\pi\sigma^*$ conversion is the fastest (eq 3, Computational Methods). However, while the $^1\pi\sigma^*/^1L_a$ crossing point coincides with the energy transition state (TS) on $^1\pi\sigma_{N9H}$* (TS$\pi\sigma_{N9H}$*) and occurs at 5.61 eV (see Table S7 of SI and Figure 3), it occurs at lower energy than the TS on

Table 6. Computed,[a] Scaled,[b] and Corrected[c] $\pi\sigma_{NH}^*$ Energies, for the Critical Geometries[d]

	$\pi\sigma_{N9H}^*$			$\pi\sigma_{N10H}^*$			L_a		
	com[a]	scal[b]	corr[c]	com[a]	scal[b]	corr[c]	com[a]	scal[b]	corr[c]
E_{vert}	5.90	5.39	5.19	5.71	5.20	5.00	5.49	4.98	4.98
E_{min}	5.55	5.04	4.84	5.37	4.86	4.66			
E_{cr}	5.61	5.10	4.90	5.64	5.13	4.93			
E_{TS}	5.61	5.10	4.90	6.03	5.52	5.32			

[a] Computed energies bay CASSCF//CASPT2/6-31+g**. [b] Energies corrected by 0.51 eV, corresponding to the difference between the computed and the experimental ^1L_a excitation energy (4.98 eV, ref 1). [c] Corrected energies by zero point energy of N−H stretch oscillators ($h\nu/2 = 0.2$ eV). [d] The S_0 equilibrium (vert) at the $\pi\sigma_{NH}^*$ minimum (min), at the $^1L_a/^1\pi\sigma_{NH}^*$ curve crossing (cr), and at $^1\pi\sigma_{NH}^*$ TS (TS).

$^1\pi\sigma_{N10H}^*$ (TS$\pi\sigma_{N10H}$ *), 5.64 and 6.03 eV, respectively (see Table S7 of SI and Figure 4). The quite different energy barriers of N_9−H and N_{10}−H have been noted also by Perun et al.[11]

It follows that, according to the *computed energies*, N−H photocleavage on $^1\pi\sigma_{N9H}^*$ ($^1\pi\sigma_{N10H}^*$) can only occur if the molecule is excited at the energy of 5.61 eV (6.03 eV) above S_0, see Table 6 and S7 of SI.

To determine the experimental energies at which the N−H photocleavage can occur, we assume that the vertical excitation of ^1L_a calculated at 5.49 eV corresponds to the maximum of the absorption band (4.98 eV)[1] and apply to all the calculated energies the correction of −0.51 eV. To these scaled energies we add the N−H zero-point-energy, which amounts to 0.2 eV for S_0 and ^1L_a, but is negligible for $^1\pi\sigma_{NH}^*$ states: actually, as we prefer to choose as zero-energies vibronic rather than electronic energies, we subtract the 0.2 eV energy from the $^1\pi\sigma_{NH}^*$ states. These critical $^1\pi\sigma_{NH}^*$ energies are collected in Table 6 together with the ^1L_a vertical energy.

By comparison, the energy of the lowest $^1\pi\sigma_{NH}^*/^1L_a$ CI was previously computed at about 5.3 eV[11,15] and the $^1\pi\sigma_{N9H}^*$ ($^1\pi\sigma_{N10H}^*$) energies at the local minimum were estimated 4.90 (4.91) eV.[12]

When the corrected energies are used (Table 6), the vertical excitation of ^1L_a (4.98 eV) provides an energy sufficient to reach the energy of the $^1L_a/^1\pi\sigma_{N9H}^*$ crossing (4.9 eV) and $^1\pi\sigma_{N9H}^*$ TS (4.9 eV) and, thus, the N_9−H photocleavage appears feasible on energy ground. On the contrary, the transition state as well as the $^1L_a/^1\pi\sigma_{N10H}^*$ crossings for the N_{10}−H curve are not accessible with the same 4.98 eV excitation, and thus, the N_{10}−H dissociation at this energy is not feasible. Only if a larger vibrational energy excess (by ca. 0.5 eV) is available, the N_{10}−H bond can be dissociated.

Although N_9−H photocleavage is feasible on energy ground exciting above 4.98 eV, it can occur with appreciable yield only if the $^1L_a \rightarrow ^1\pi\sigma_{N9H}^*$ internal conversion is fast and can compete with the dominant ^1L_a relaxation along its MEP ($k_1 = 10^{13}$ s^{-1}).

The $^1L_a \rightarrow ^1\pi\sigma_{N9H}^*$ IC occurs with a rate constant of $k = 10^{13}F$ s^{-1}, where F is the total Franck−Condon factor, which is the product of the F_i factors of individual normal modes. Most of the normal modes will have similar frequencies and equilibrium geometries in the two states and each will have $^1L_a/^1\pi\sigma_{N9H}^*$ F_i factors close to 1. The N−H stretch and the ring puckering (^1L_a MEP) oscillators have different potential energy profiles in the two states, and therefore, their $^1L_a/^1\pi\sigma_{N9H}^*$ F_i factors are expected to be very small if a modest vibrational energy is available. Thus, the quantum yield of N_9−H photocleavage process can be estimated to be negligible when exciting ^1L_a at 5 eV, because the rate of the $^1L_a \rightarrow ^1\pi\sigma_{N9H}^*$ IC will be orders of magnitude slower than the rate of Ade relaxation along the ^1L_a MEP. The FC factor and rate of

Scheme 2

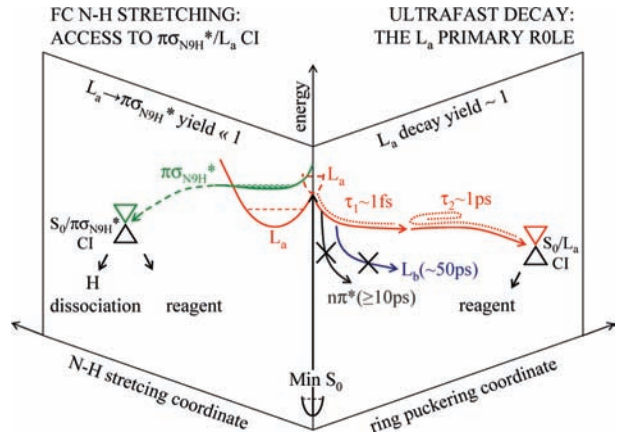

$^1L_a \rightarrow ^1\pi\sigma_{N9H}^*$ are expected to become larger as the excitation energy increases by a fraction of eV above the threshold. These results are lower than the energies computed earlier[15] (6.2 eV), agree with the findings that the lower excitation energy for obtaining N−H photocleavage by exciting the ^1L_a absorption band is ≈5.32 eV.[47]

4. Conclusions

We have analyzed, by CASPT//CASSCF calculations and by examining the pertinent experimental data, the decay paths (and their efficiency) of the lowest electronic excited states of Ade ($^1n\pi^*$, ^1L_b, and ^1L_a), including $^1L_a \rightarrow ^1\pi\sigma_{NH}^*$ internal conversion.

In summary, the results are the following: (i) $^1n\pi^*$ and ^1L_b states decay with lifetimes longer than 10 ps, returning to the ground state without giving photoproducts. The $^1n\pi^*$ state decays mainly via ISC to a quasi-degenerate $^3\pi\pi^*$ triplet state. (ii) The observed biexponential decay with 0.1 and 1 ps lifetimes is attributed solely to ^1L_a: the faster decay to the in-plane vibrational relaxation plus a ring puckering deformation, and the slower one to the exiting from a plateau induced by the out-of plane N_2−H bending, leading to the S_0/L_a CI (Scheme 2). (iii) ^1L_a internal conversion to $^1n\pi^*$ and ^1L_b states occurs with negligible yield. (iv) The above results are in agreement with and explain features of supersonic beams spectra, gas phase TRPES spectra and of the time-resolved fluorescence spectra in water solution. (v) N_9−H and N_{10}−H photocleavages are found possible (albeit with a very low quantum yield) for excitation energies ≥5 eV in the case of N_9−H and ≥5.5 eV for N_{10}−H. Their quantum yields are governed by the FC factors of the $^1L_a \rightarrow ^1\pi\sigma_{NH}$ internal conversion.

Acknowledgment. The support by funds from MURST PROGETTO PRIN E.F. 2007 Prot 2007NZLYE5 "Trasferimenti di energia, carica e molecule in sistemi complessi" is gratefully acknowledged.

Supporting Information Available: Cartesian coordinates of all the structures discussed in the text (data in Å); absolute energy of all calculated structures (data in Hartrees); N−H dissociation path energy values; vibrational frequencies used in the RRKM calculation; evaluation of $h\nu_{NH}/2$ corrections for the quantization of the N_9−H stretch vibration in S_0, L_a, and $\pi\sigma_{N9H}^*$ states; gradient difference (GD) and derivative coupling (DC) vectors of L_a/L_b and $L_a/n\pi^*$ CIs; and complete refs 60 and 61. This material is available free of charge via the Internet at http://pubs.acs.org.

JA902311Y